frontiers

Supplementary Material

Table S1 – Satellite altimetry missions used for the assessment of the Mediterranean Sea wave hindcast, with information on the dataset.

	Start date	End date	Number of collocations
ERS-1	01/08/1991	02/06/1996	377951
ERS-2	29/04/1995	11/05/2009	1009321
JASON-1	15/01/2002	20/06/2013	1117396
JASON-2	04/07/2008	30/09/2019	1261700
JASON-3	12/02/2016	31/12/2019	519229
CRYOSAT-2	14/07/2010	31/12/2019	951376
ENVISAT	14/05/2002	08/04/2012	674344
SENTINEL-3A	01/03/2016	31/12/2019	476303

Table S2 – Spatial averages over the MS and sub-basins of the 50th and 99th percentile $\overline{C}_{max}$ trends shown in Figure S10 (cm decade^{-1}), during 1981-2019 summer and winter seasons. Averages over the points where the trends are significant (black dots in Figure S10; tested with Mann-Kendall test and 90% confidence interval) and over all the points. Value between parentheses is the percentage of points with statistically significant trends in a (sub-) basin with respect to all the points in the (sub-) basin.

	50th percentile				**99th percentile**			
	summer		winter		summer		winter	
	significant	all	significant	all	Significant	all	significant	all
Mediterranean	**-1.1 (23.3%)**	**-0.6**	**1.5 (2.5%)**	**0.4**	**-2.6 (25.7%)**	**-0.4**	**8.7 (4.9%)**	**1.2**
Adriatic	0.8 (3.5%)	0.4	2.9 (27.0%)	2.0	-8.7 (17.2%)	-3.0	8.3 (6.6%)	0.7
Ionian	0.4 (17.0%)	-0.5	-1.7 (0.1%)	-0.9	10.9 (28.1%)	5.5	-5.9 (0.1%)	-0.3
Tyrrhenian	-1.7 (4.3%)	-0.5	2.6 (0.1%)	1.2	-10.0 (4.5%)	0.2	-11.7 (6.8%)	-4.2
Levantine	-1.6 (54.4%)	-1.0	-2.5 (2.2%)	-0.7	-8.9 (43.1%)	-4.1	14.5 (10.2%)	5.1
Western	1.1 (0.8%)	-0.5	3.6 (1.6%)	2.8	-8.0 (9.6%)	-2.1	0.8 (2.0%)	0.1

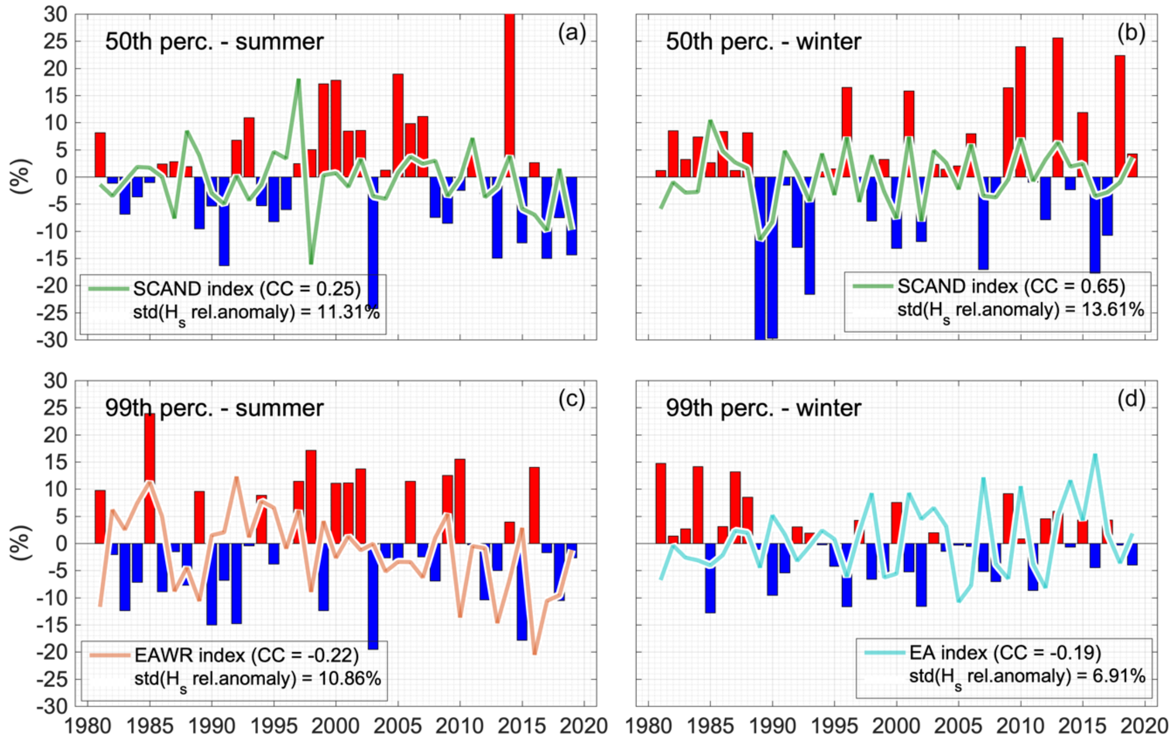

Figure S1 - Inter-annual variability of typical and extreme wind-wave climate in the Tyrrhenian Sea (1981-2019). Relative anomaly of 50^th^ (panels a-b) and 99^th^ (panels c-d) percentiles of H_s during winter and summer seasons, spatially averaged over the Tyrrhenian Sea. Solid lines represent the most correlated teleconnection indices among NAO, EA, EAWR and SCAND (correlation coefficient CC in the legend; indices are magnified ten times for graphical purposes).

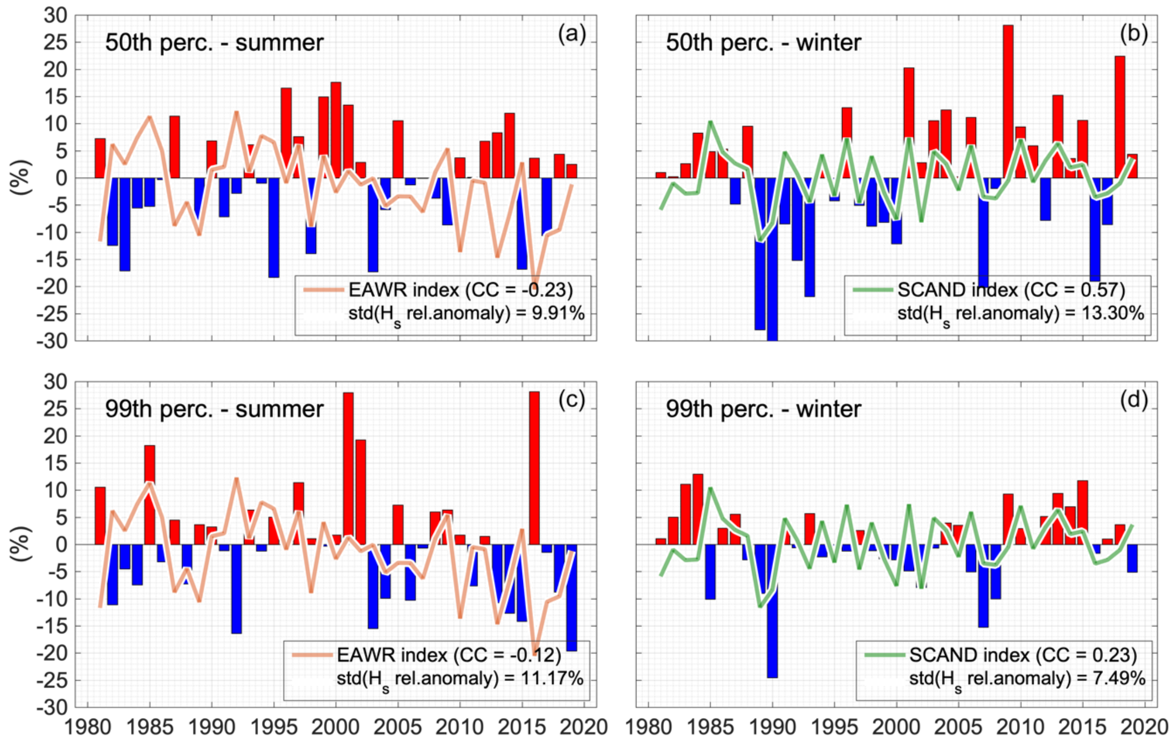

Figure S2 - Inter-annual variability of typical and extreme wind-wave climate in the Adriatic Sea (1981-2019). Relative anomaly of 50th (panels a-b) and 99th (panels c-d) percentiles of H_s during winter and summer seasons, spatially averaged over the Adriatic Sea. Solid lines represent the most correlated teleconnection indices among NAO, EA, EAWR and SCAND (correlation coefficient CC in the legend; indices are magnified ten times for graphical purposes).

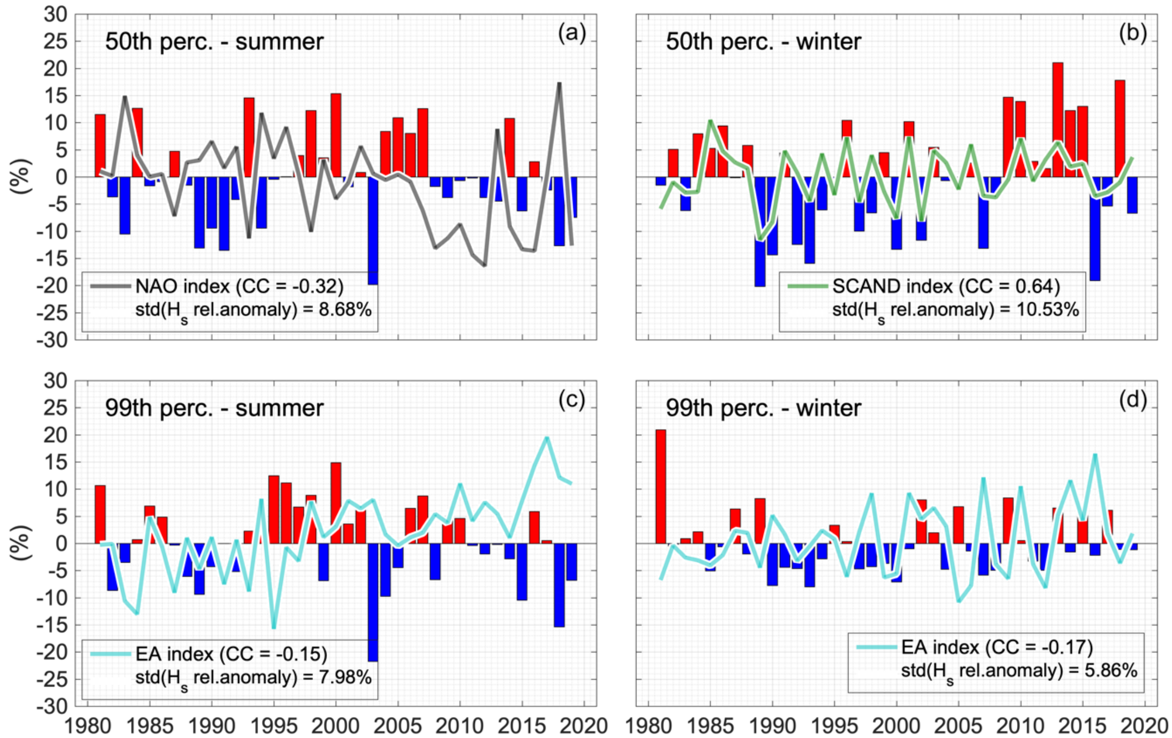

Figure S3 - Inter-annual variability of typical and extreme wind-wave climate in the Western Mediterranean Sea (1981-2019). Relative anomaly of 50th (panels a-b) and 99th (panels c-d) percentiles of H_s during winter and summer seasons, spatially averaged over the Western Mediterranean Sea. Solid lines represent the most correlated teleconnection indices among NAO, EA, EAWR and SCAND (correlation coefficient CC in the legend; indices are magnified ten times for graphical purposes).

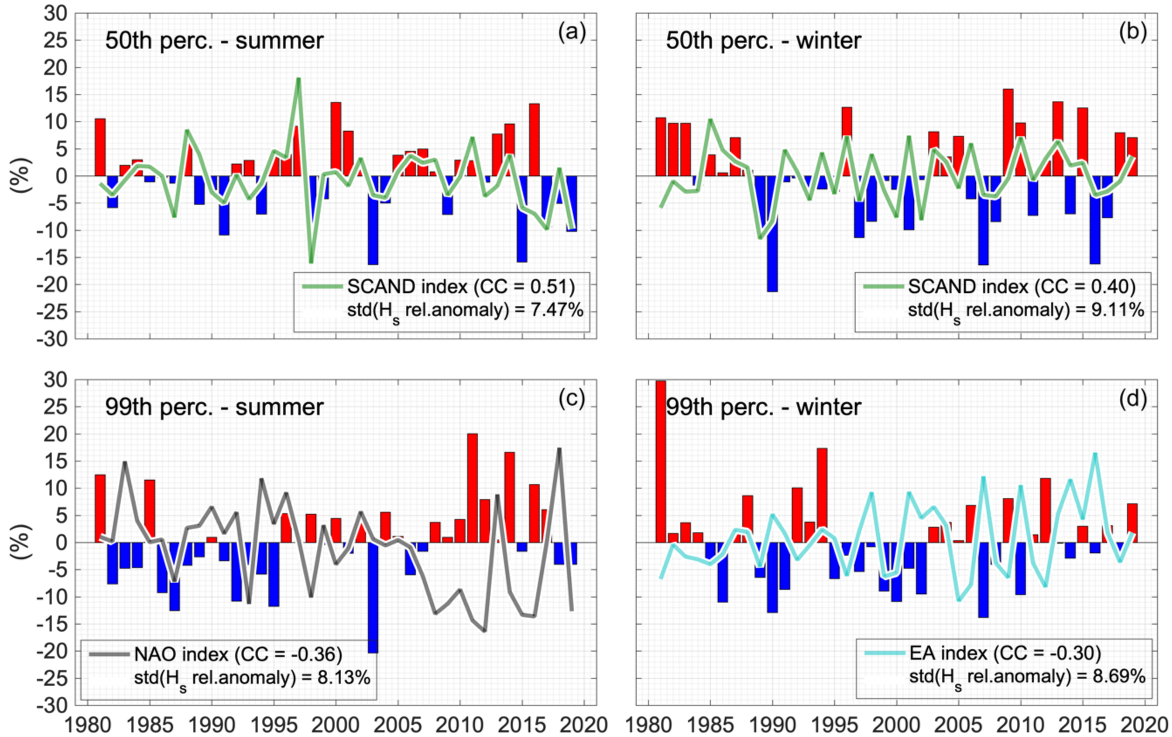

Figure S4 - Inter-annual variability of typical and extreme wind-wave climate in the Ionian-Meridional Sea (1981-2019). Relative anomaly of 50th (panels a-b) and 99th (panels c-d) percentiles of H_s during winter and summer seasons, spatially averaged over the Ionian-Meridional Sea. Solid lines represent the most correlated teleconnection indices among NAO, EA, EAWR and SCAND (correlation coefficient CC in the legend; indices are magnified ten times for graphical purposes).

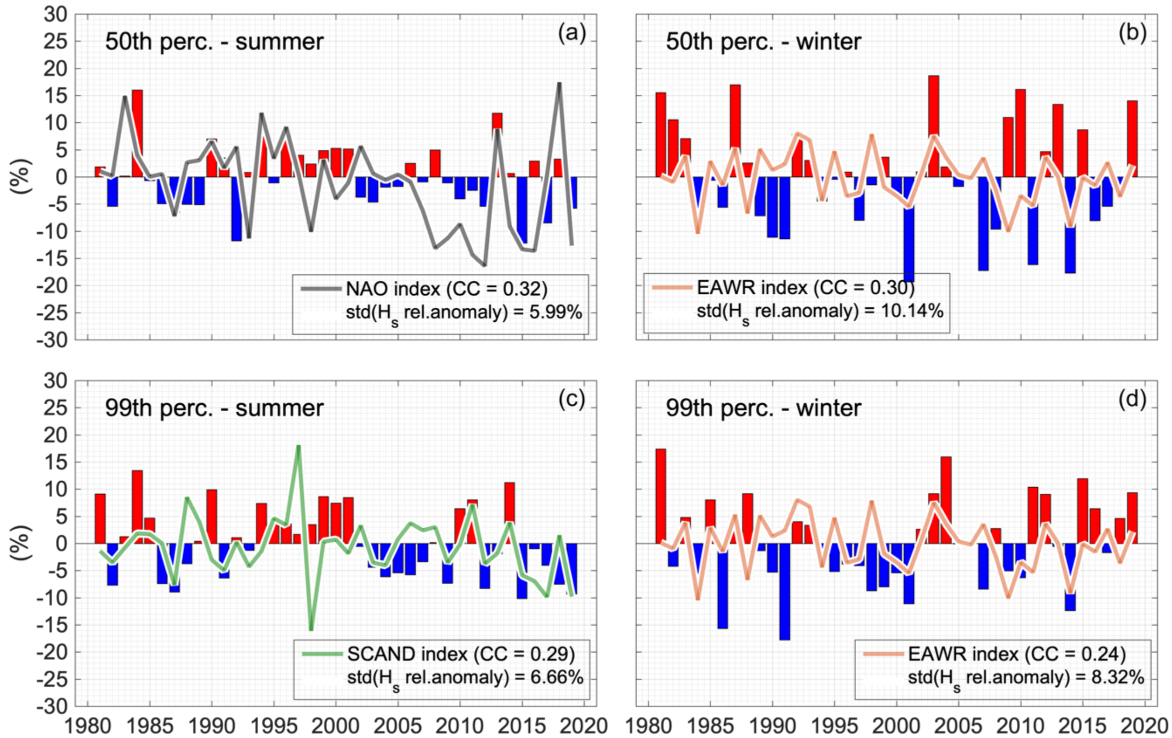

Figure S5 - Inter-annual variability of typical and extreme wind-wave climate in the Levantine-Aegean Sea (1981-2019). Relative anomaly of 50th (panels a-b) and 99th (panels c-d) percentiles of H_s during winter and summer seasons, spatially averaged over the Levantine-Aegean Sea. Solid lines represent the most correlated teleconnection indices among NAO, EA, EAWR and SCAND (correlation coefficient CC in the legend; indices are magnified ten times for graphical purposes).

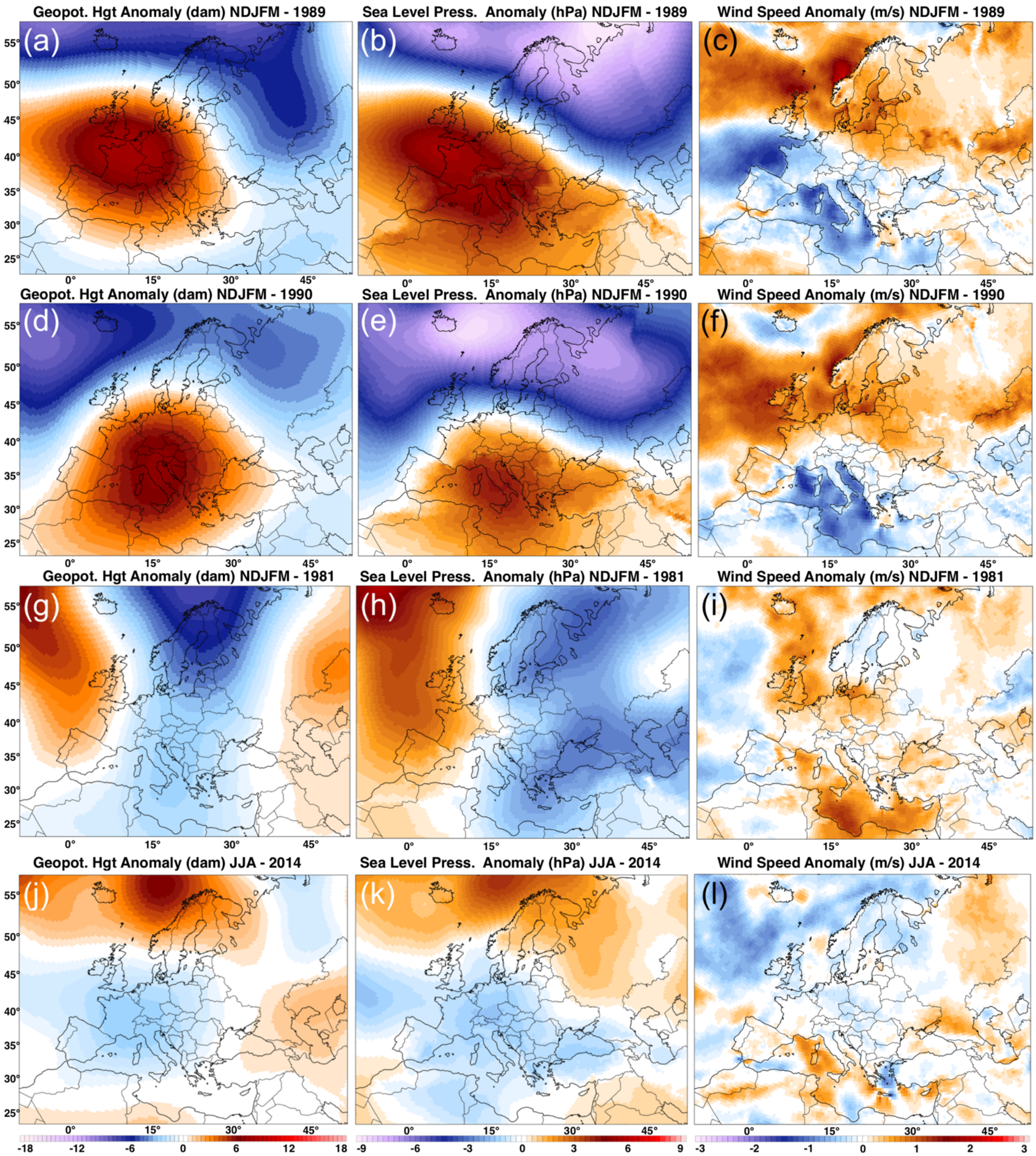

Figure S6 – Anomalies of atmospheric parameters when the largest wave anomalies occurred: geopotential height at 500 hPa (dam; panels a, d, g, j), sea level pressure (hPa; panels b, e, h, h), and wind speed at 10 meters (m/s, panels c, f, i, l), for winter 1989, winter 1990, winter 1981 and

summer 2014. Data based on the ERA5 dataset. Source of the images is https://climatereanalyzer.org, produced by Climate Change Institute, University of Maine.

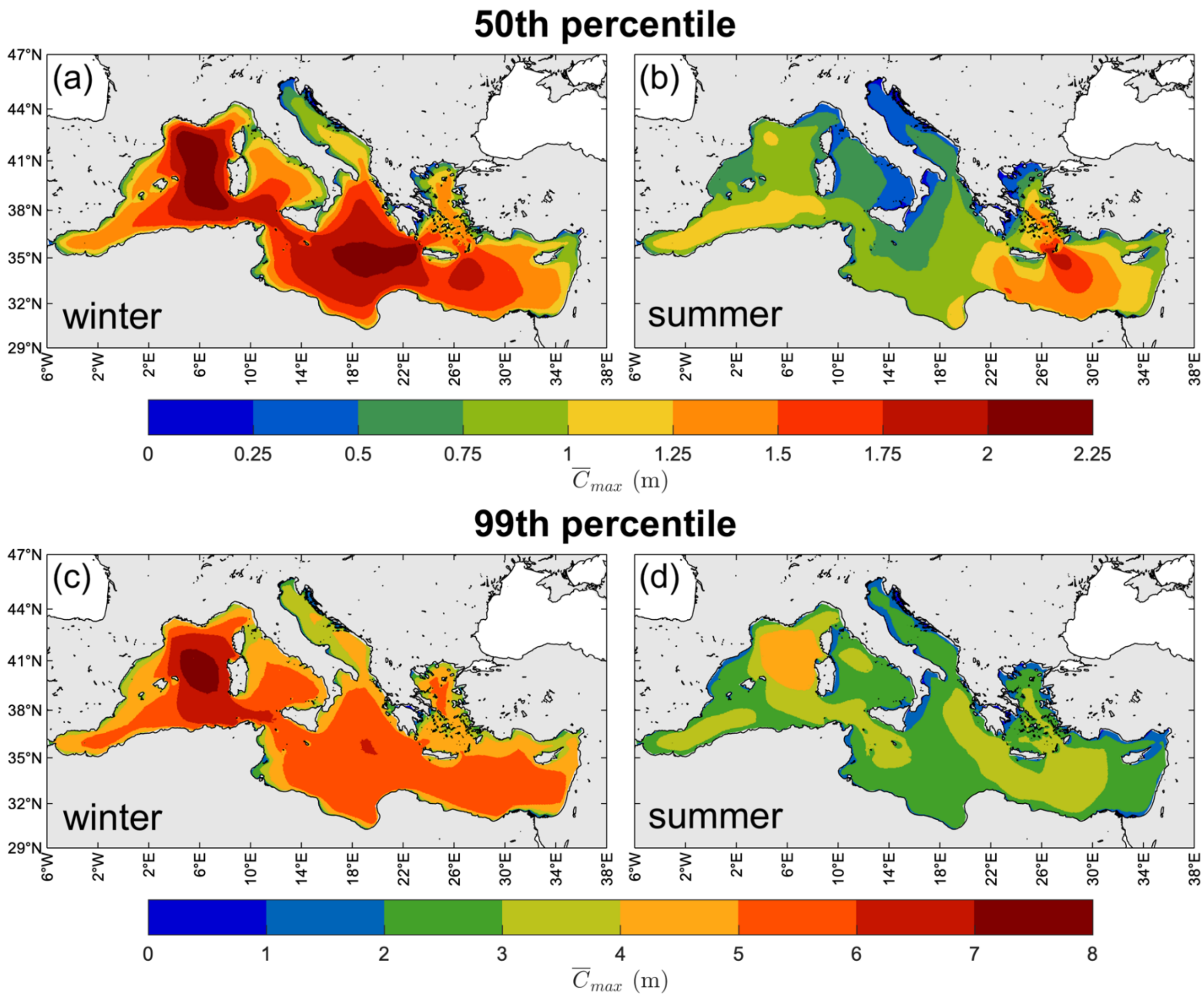

Figure S7 – Climate of the maximum individual waves. Yearly-averaged seasonal 50th (panels a-b) and 99th (panels c-d) percentiles of $\overline{H}_{max}$ (1981-2019): winter (NDJFM, panels a, c), summer (JJA, panels b, d).

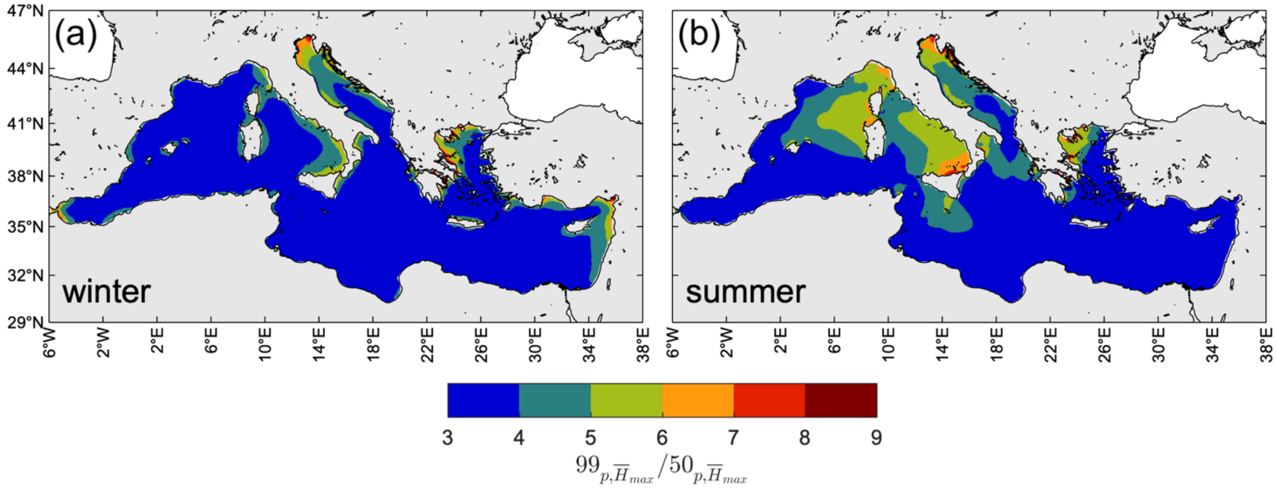

Figure S8 – Intra-seasonal variability of maximum individual wave climate. Yearly-averaged ratio of the 99th to 50th percentile of $\overline{H}_{max}$ (1981-2019), during winter (NDJFM, panel a) and summer (JJA, panel b).

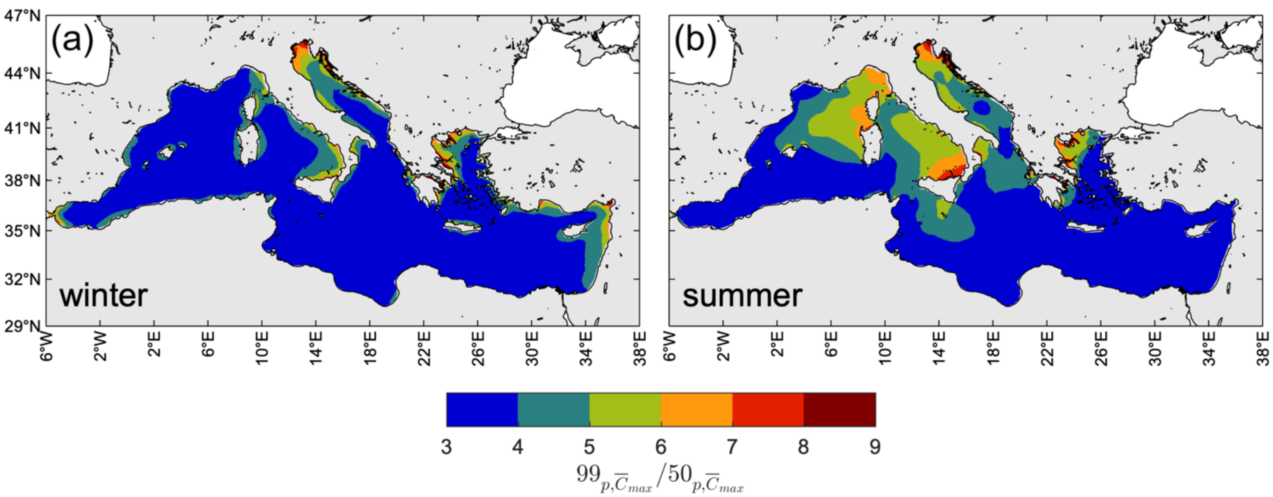

Figure S9 – Intra-seasonal variability of maximum individual wave climate. Yearly-averaged ratio of the 99th to 50th percentile of $\overline{C}_{max}$ (1981-2019), during winter (NDJFM, panel a) and summer (JJA, panel b).

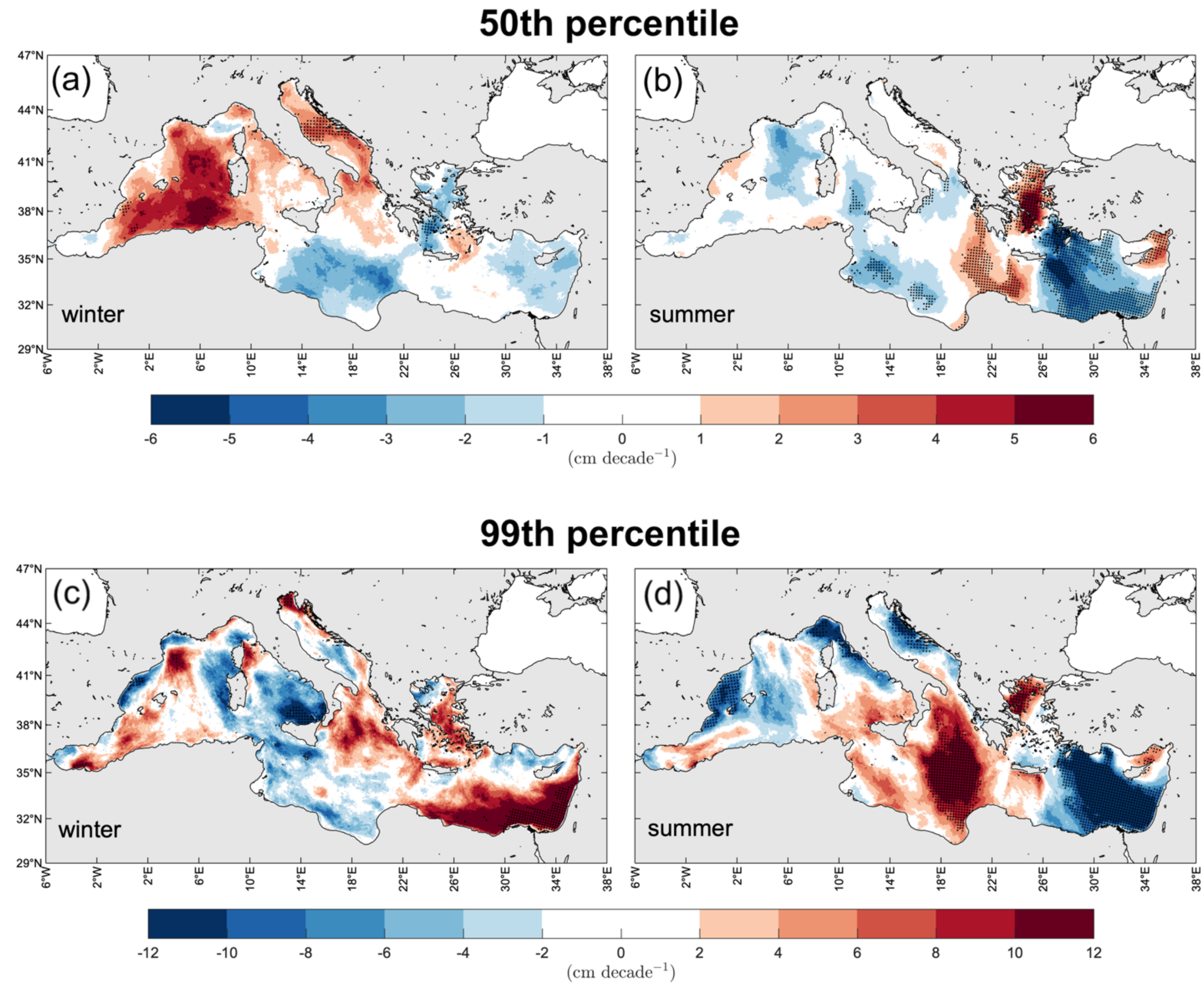

Figure S10 – Change of the MS typical (50th percentile, panels a-b) and extreme (99th percentile, panels c-d) wind-wave climate. Trend of the winter (panels a, c) and summer (panels b, d) $\overline{C}_{max}$ during 1981-2019. Statistically significant trends at the 90% confidence intervals are denoted by (decimated for graphical purposes) black dots.